Publishing Excellence
Inspiring Progress
ARISTON PUBLICATIONS

Science of Alloys and Glasses

ISSN: 3143-0732 https://aristonpubs.com/journal/science-of-alloys-and-glasses https://doi.org/10.69626/sag.2025.0135

RESEARCH ARTICLE

# Radiation Shielding Properties of $Er_2O_3$–Doped Tellurite Heavy Metal Oxide Glasses for Medical Radiation Applications

**Al-Anoud T. Al Ahmari [1], Bayan Aljuwaybiri [2,*]**

**ABSTRACT:** A series of erbium oxide ($Er_2O_3$)-doped tellurite heavy metal oxide glasses with the composition $62TeO_2$–$5K_2TeO_3$–$20ZnO$–$10Nb_2O_5$–$3PbF_2$–$xEr_2O_3$ (x = 2, 3, and 4.5 mol%) were developed and examined to assess their suitability for radiation shielding applications. The gamma-ray attenuation performance was analyzed across a wide photon energy range using essential shielding parameters such as the linear attenuation coefficient (LAC), mass attenuation coefficient (MAC), half-value layer (HVL), tenth-value layer (TVL), mean free path (MFP), and effective atomic number ($Z_{eff}$). The findings indicate that incorporating $Er_2O_3$ improves the glass system's radiation attenuation. This improvement is associated with increases in density and atomic number, which enhance the probability of photon interaction. As a result, higher attenuation coefficients and lower penetration-related parameters were observed, confirming the effectiveness of erbium incorporation in strengthening the shielding performance. The prepared glasses showed particularly strong attenuation behavior within photon energy ranges relevant to diagnostic imaging. These results demonstrate that $Er_2O_3$-doped tellurite glasses offer a promising combination of radiation-shielding efficiency, making them suitable candidates for medical radiation protection applications.

**Keywords:** Tellurite glass; erbium oxide; radiation shielding; attenuation coefficient; effective atomic number; medical radiation protection

**Received: 18 January 2025; Revised: 29 March 2025; Accepted: 03 June 2025; Published Online: 17 June 2025**

## 1. INTRODUCTION

Ionizing radiation plays a significant role in a variety of applications, including medicine, nuclear power, research, and manufacturing. Its contribution to medicine has demonstrated extensive applications in both diagnosis and treatment. On the other hand, ionizing radiation can be harmful to human health if precautions are not taken. Organ and cell damage resulting from ionizing radiation exposure can cause cancer at lower levels over a longer period, and high acute doses can cause radiation burns and sickness [1].

[1] Department of Physics, Faculty of Science, King Khalid University, AlQuraa, Abha, P. O. Box 906, Kingdom of Saudi Arabia.
[2] De Armed Forces hospitals-Taif Region Taif, Kingdom of Saudi Arabia.

* Author to whom correspondence should be addressed: Bayanomar275@gmail.com (B. Aljuwaybiri)

Lead is the most commonly used shielding material due to its high atomic number and density. Various types of radiation, especially X-rays and gamma rays, can be effectively attenuated by lead [2]. However, lead has several drawbacks, including low mechanical strength and chemical instability, as well as its high cost [3]. Seeking a substitute to lead to a shared objective, such as polymers, glass, and alloys, which have exceptional density, transparency, and low toxicity. Recently, there has been considerable interest in using heavy-metal oxide glasses for radiation shielding, including boron, tellurium, barium, and silicon oxides [4, 5]. These glasses could replace conventional concrete as gamma-ray and X-ray shielding materials, according to some research. Oxide-based glasses are suitable for many medical imaging applications due to their interesting properties. Most glasses are thermally stable, have a low glass transition temperature, low crystallization ability, moderate physical and chemical

© Ariston Publications 2025. All rights reserved.

resistance, and a low melting point [6, 7]. Due to its excellent thermal stability, high density, electrical conductivity, and corrosion resistance, tellurite is a glass intermediate with significant promise for radiation shielding. Furthermore, this type of glass can be stable when modified [8].

In this paper, we examined a tellurite glass system doped with heavy metal oxides for shielding purposes. We investigated $62TeO_2$-$5K_2TeO_3$-$20ZnO$-$10Nb_2O_5$-$3PbF_2$ glasses doped with different amounts of erbium oxide (x mol % $Er_2O_3$, x=2, 3, 4.5). To investigate the shielding properties, several shielding parameters have been used, like the linear attenuation coefficient and mass attenuation coefficient LAC and MAC, the half-value layer, mean free path MFP, $Z_{eff}$, and tenth value layer TVL. On the other hand, the spectroscopic properties were investigated with the JO theory based on the absorption spectra.

## 2. EXPERIMENTAL DETAILS

### 2.1. Sample preparation

A series of tellurite glasses with the composition $64TeO_2$-$5K_2TeO_3$-$20ZnO$-$10Nb_2O_5$-$3PbF_2$, doped with 2, 3, and 4.5 mol % of $Er_2O_3$, were prepared from high-purity raw materials using the quench-melting technique. All the batches were placed in a gold crucible and heated inside an electric furnace at 950 °C for 30 min. Then, the melt was quenched in a graphite mold and preheated at 340 °C for two hours. The thickness of the polished glass was L = 0.381 cm. The densities were measured using a helium pycnometer (AccuPyc 1330) with an accuracy of ±0.0003% (see Table 1). Adding transition–metal oxides, such as erbium oxides, as network modifiers has increased the formation of non-bridging oxygen, thereby raising the glass density. Sample D shows the highest density among the glass system samples, which may be attributed to the $Er_2O_3$ concentration. The absorption spectra of the prepared glasses were recorded over the wavelength range of 300 nm to 2000 nm using a JASCO V-570 spectrophotometer UV/VIS/NIR.

### 2.2. Glass characterizations

The efficacy of shielding material can be determined by its physical properties and radiation-shielding parameters, the most significant of which are the scattering and absorption cross sections, the effective atomic number Zeff, the electron density, and the HVL. The cross-section is characterized by the total MAC (μ/ρ). Mass attenuation coefficient MAC (μ/ρ) is equivalent to the linear attenuation coefficient divided by the density of the absorber (μ/ρ) and is expressed in $cm^2/g$ [9]. MAC can be calculated by the following formula:

$$\frac{\mu}{\rho} = \sum_i \omega_i \left(\frac{\mu}{\rho}\right) i \qquad (1)$$

Where $\omega_i$ is the fraction by weight of the $i^{th}$ atomic element, and $\frac{\mu}{\rho}$ is the MAC of the $i^{th}$ atomic element. Linear attenuation coefficient μ is a constant that defines the fraction of attenuation of incident photons in a mono-energetic beam per unit thickness of a material. It includes all possible interactions, including coherent, Compton, and photoelectric scattering. It is expressed numerically in units of $cm^{-1}$. The linear attenuation coefficient increases with the atomic number and density of the absorbing material and decreases with photon energy [10]. The coefficient μ can be calculated using the formula [11]:

$$\mu = \frac{\ln(\frac{I_0}{I_x})}{x} . \qquad (2)$$

The Mean free path MFP is the average distance between two successive interactions.

$$MFP = \frac{1}{\mu} \qquad (3)$$

## 3. RESULTS AND DISCUSSION

The computed LACs and MACs of the prepared samples at energies between 0.015 MeV and 15 MeV are shown in Figure 1 and Figure 2. Photoelectric and Compton scattering, the two main interactions in the diagnostic energy range, are responsible for the reduction in attenuation coefficients with increasing photon energy. The superiority of the mass attenuation of sample D was due to the higher amount of heavy metal oxide material that was doped. Samples B and C, which contained erbium oxide ($Er_2O_3$), showed slightly higher MAC and LAC values. Otherwise, sample A and the undoped sample recorded slightly lower values. As shown in Figure 2, the LACs of sample D were superior to those of the other samples in all energies due to the sample's higher density (Table 1). For example, the value of LACs recorded for sample D was 264.447 $cm^{-1}$, compared to 232.519 $cm^{-1}$ (sample A), 246.859 $cm^{-1}$ (sample B), and 253.739 $cm^{-1}$ (sample C) at 0.15 MeV.

MFP is the average distance between successive interactions; the lower the MFP, the more effective the shielding material. Figure 3 demonstrates the MFP as a function of the photon energy of the samples. The glass sample doped with higher erbium oxide showed the lowest MFP, consistent with its HVL, as both are strongly dependent on the attenuation coefficient. Therefore, at 0.15 MeV, the MFP of the sample D was 0.003778 cm, compared to 0.00941 cm, 0.00405 cm, and 0.0043 cm, respectively. Furthermore, the MFPs of the samples were compared with other shielding materials like (RS-253 G18, RS-360, and RS-520), as shown in Figure 3. Similar findings to the HVLs were observed: the higher the density and photon attenuation of the shielding material, the lower the MFP.


© Ariston Publications 2025. All rights reserved.

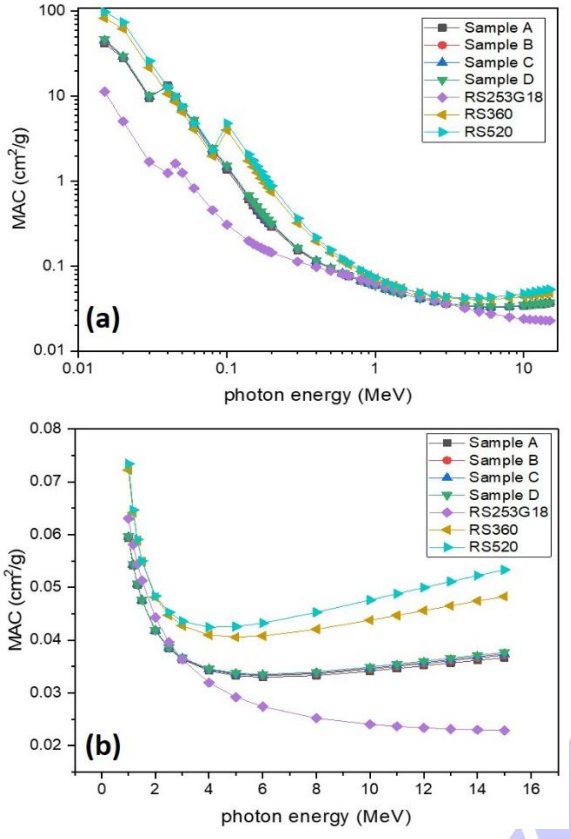



**Fig. 1.** MAC of the samples in a range of (a) 0.18-15 Mev, (b) 1-15 Mev.

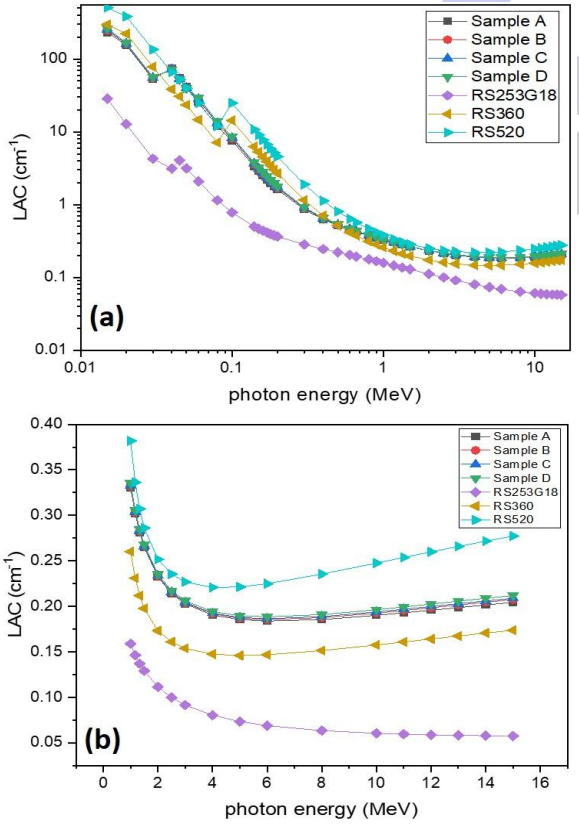



**Fig. 2.** LAC of samples with a range of (a) 0.18-15 MeV, (b) 1-15 MeV.

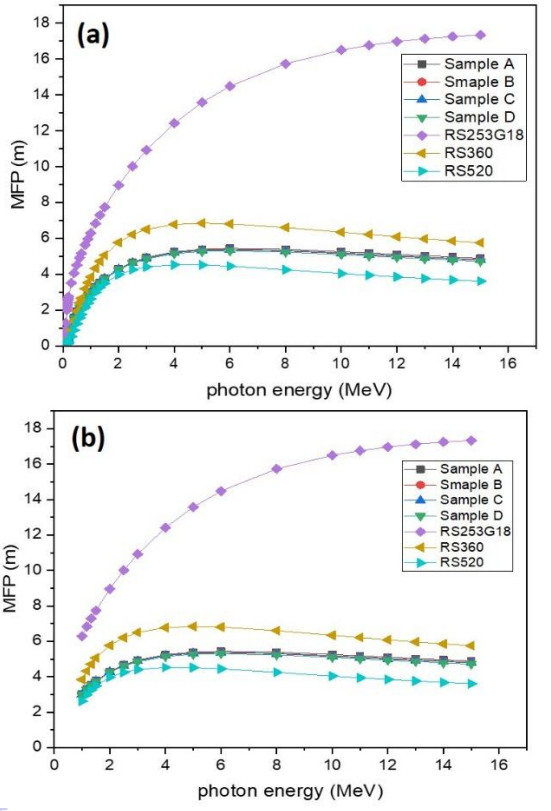



**Fig. 3.** MFP of the samples with a range of (a) 0.18-15 Mev, (b) 1-15 MeV.

The choice of shielding material for a given application depends on the Half Value Layer (HVL), which is the thickness of the shielding material that reduces the intensity of gamma rays to half their initial value. The Tenth Value Layer (TVL) is another shielding parameter, similar to HVL, which represents the thickness of shielding material required to reduce gamma-ray intensity to one-tenth of its original value [12]. The critical parameters can be calculated by [13]:

$$HVL = \frac{In2}{LAC} \tag{4}$$

$$TVL = \frac{In10}{LAC} \tag{5}$$

These parameters depend on the material type, radiation type, and radiation energy. The TVL is illustrated in Figure 4. It has been observed that TVL values gradually increase with photon incidence, and the variation in TVL across these samples reflects the dominance of different photon-interaction mechanisms.

The interaction between gamma rays and glass samples, along with energy variation, was as follows: pair production dominates at high energies above 1.022 MeV, Compton scattering dominates in the intermediate energy range, and photoelectric scattering dominates at low energies [12].

© Ariston Publications 2025. All rights reserved.

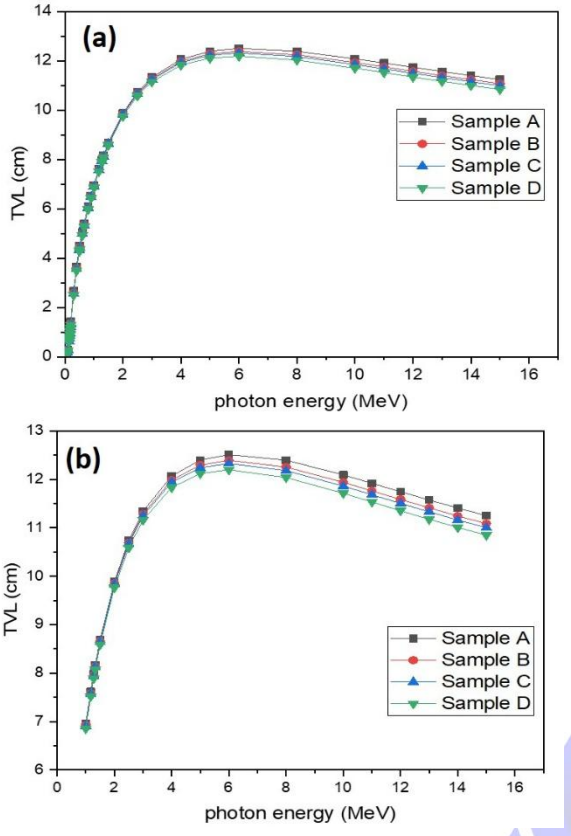



**Fig. 4** The tenth value layer (TVL) of the glass samples (a) from 0.18 to 15 MeV, (b) from 1 to 15 MeV.

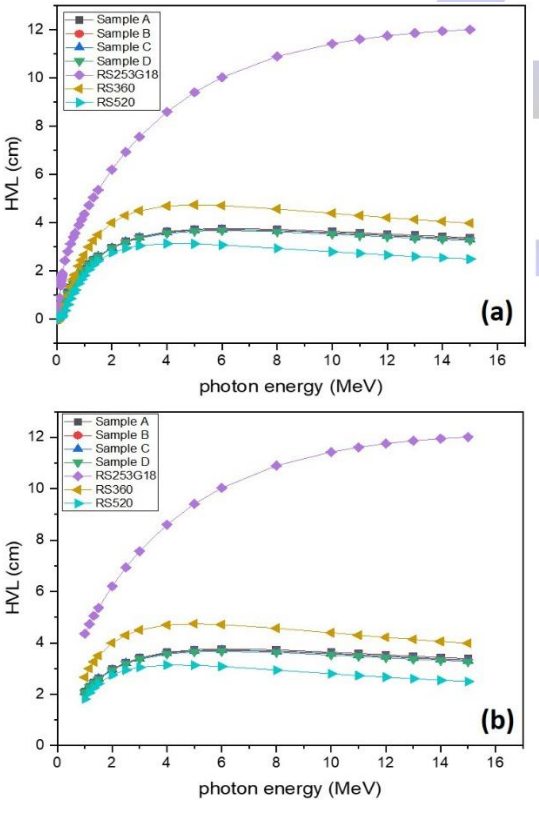



**Fig. 5.** The half value layer (HVL) of the glass samples compared with the standard materials at photon energy (a) from 0.18 to 15 MeV, (b) from 1 to 15MeV.

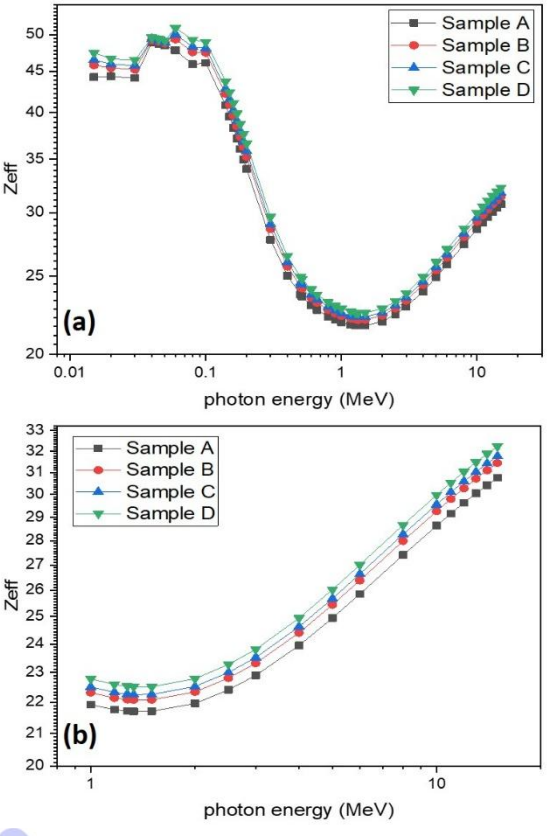



**Fig. 6 (a b).** Effective atomic number of glass samples with photon energy.

The TVL of all samples decreases rapidly at 8 MeV due to the predominance of the photoelectric effect, whereas the HVL increases slowly at 1.02 MeV due to pair production. The undoped sample has the highest HVL among the prepared samples at 6 MeV, whereas sample D has the lowest, which is preferred for gamma-ray shielding, as photon incidence on the material is higher when these parameters are low.

The prepared samples have been compared with the standard materials (RS253G18–RS360–RS520) using the HVL parameter. It is observed that all samples considered have consistently lower values than the (RS253G18- RS360) standard materials due to the predominance of Compton scatter at photon energies from 8 to 15 MeV. Contrary to the (RS520) standard material, which records the lowest HVL, preferred for our shielding. Therefore, the HVL of the (RS253G18) standard material increases gradually as it crosses the 2 MeV threshold, indicating the presence of pair production.

The photon interaction with the glass samples can also be affected by the effective atomic number, which is the number of electrons surrounding the nucleus. The formula to calculate the effective atomic number is as follows [14]:

$$Z_{eff} = \frac{\sigma_a}{\sigma_e} \quad (6)$$


© Ariston Publications 2025. All rights reserved.

**Table 1**. The compositions, density, and molar volume of the glass samples.

| Glass sample | $TeO_2$ | $K_2TeO_3$ | ZnO | $Nb_2O_5$ | $PbF_2$ | $Er_2O_3$ | Density (g/cm$^3$) | $V_M$ (cm$^3$ /mol) |
|---|---|---|---|---|---|---|---|---|
| **Sample A** | 62 | 5 | 20 | 10 | 3 | 0 | 5.5713 | 29.05 |
| **Sample B** | 62 | 5 | 20 | 10 | 3 | 2 | 5.5816 | 29.77 |
| **Sample C** | 62 | 5 | 20 | 10 | 3 | 3 | 5.5901 | 30.10 |
| **Sample D** | 62 | 5 | 20 | 10 | 3 | 4.5 | 5.6214 | 30.48 |

The $Z_{eff}$ values of the prepared glasses are shown in Figure 6. Figure 6(a) shows a rapid decrease in $Z_{eff}$ values for all the samples as photon energy increases and illustrates that sample D recorded the highest $Z_{eff}$ value at 0.06 MeV, which is favorable for our shielding. Contrary to the threshold 2 MeV, its rapid increase is due to the predominance of the pair production process. Sample D has the highest $Z_{eff}$ value, while sample A has the lowest. Figure 6(b) illustrates that all the samples recorded a rapid increase in $Z_{eff}$ values due to the photoelectric process.

## 4. CONCLUSIONS

A series of $Er_2O_3$-doped tellurite glass samples with the composition $62TeO_2–5K_2TeO_3–20ZnO–10Nb_2O_5–3PbF_2–xEr_2O_3$ (x = 0, 2, 3, and 4.5 mol%) were successfully prepared and evaluated over a wide photon energy range. The obtained results showed that increasing the $Er_2O_3$ content improved the shielding performance of the prepared glasses. The sample with the highest erbium concentration exhibited the highest linear and mass attenuation coefficients and effective atomic number, while the mean free path, half-value layer, and tenth-value layer decreased. This behavior is mainly attributed to the increase in density and the presence of high-atomic-number erbium ions, which enhance the probability of photon interaction within the glass matrix. The sample with the highest $Er_2O_3$ concentration demonstrated the best overall attenuation capability, particularly at low photon energies relevant to diagnostic radiation. The investigated $Er_2O_3$-doped tellurite glass system can be considered a potential alternative to conventional shielding materials for diagnostic X-ray and gamma-ray protection. Further investigations, including experimental validation and practical implementation, are recommended to support their use in medical radiation protection applications.

## DECLARATIONS

### Ethical Approval

We affirm that this manuscript is an original work, has not been previously published, and is not currently under consideration for publication in any other journal or conference proceedings. All authors have reviewed and approved the manuscript, and the order of authorship has been mutually agreed upon.

### Funding

Not applicable

### Availability of data and material

The datasets used and/or analyzed during the current study are available from the corresponding author on reasonable request.

### Conflicts of Interest

The authors declare that they have no financial or personal interests that could have influenced the research and findings presented in this paper. The authors alone are responsible for the content and writing of this article.

### Authors' contributions

All authors contributed equally in the preparation of this manuscript.

## ACKNOWLEDGMENTS

The authors extend their appreciation to University Higher Education Fund for funding this research work under Research Support Program for Central labs at King Khalid University through the project number CL/PRI/B/3.

## REFERENCES

[1] Ryan, J.L., **2012.** Ionizing radiation: the good, the bad, and the ugly. *Journal of Investigative Dermatology*, *132*(3), pp.985-993.

[2] National Committee on Radiation Protection (US), **2004.** Structural shielding design for medical x-ray imaging facilities. National Council on Radiation Protection and Measurements.

© Ariston Publications 2025. All rights reserved.

[3] Ara, A. and Usmani, J.A., **2015.** Lead toxicity: a review. *Interdisciplinary Toxicology*, *8*(2), p.55.

[4] Lakshminarayana, G., Dong, M.G., Al-Buriahi, M.S., Kumar, A., Lee, D.E., Yoon, J. and Park, T., **2020.** $B_2O_3$–$Bi_2O_3$–$TeO_2$–BaO and $TeO_2$–$Bi_2O_3$–BaO glass systems: a comparative assessment of gamma-ray and fast and thermal neutron attenuation aspects. *Applied Physics A*, *126*(3), p.202.

[5] Singh, K.J., Kaur, S. and Kaundal, R.S., **2014.** Comparative study of gamma ray shielding and some properties of PbO–$SiO_2$–$Al_2O_3$ and $Bi_2O_3$–$SiO_2$–$Al_2O_3$ glass systems. *Radiation Physics and Chemistry*, *96*, pp.153-157.

[6] Li, Q., Wei, Q., Zheng, W., Zheng, Y., Okosi, N., Wang, Z. and Su, M., **2018.** Enhanced radiation shielding with conformal light-weight nanoparticle–polymer composite. *ACS applied materials & interfaces*, *10*(41), pp.35510-35515.

[7] Schueler, B.A., **2010.** Operator shielding: how and why. *Techniques in vascular and interventional radiology*, *13*(3), pp.167-171.

[8] Özdemir, T., Güngör, A.H.M.E.T., Akbay, I.K., Uzun, H. and Babucçuoglu, Y., **2018.** Nano lead oxide and epdm composite for development of polymer based radiation shielding material: Gamma irradiation and attenuation tests. *Radiation Physics and Chemistry*, *144*, pp.248-255.

[9] Beutel, J., **2000.** *Handbook of medical imaging* (Vol. 3). SPIE Press.

[10] Huda, W. and Slone, R., **1996.** Review of radiologic physics. *Physics in Medicine and Biology*, *41*(12), p.2807.

[11] McKetty, M.H., **1998.** The AAPM/RSNA physics tutorial for residents. X-ray attenuation. *Radiographics*, *18*(1), pp.151-163.

[12] Hafiz, M.S., Othman, H.A., Kawady, N.A., Hager, I.Z., El-Feky, M.G. and El-Samman, H.M., **2021.** Structural properties and gamma rays shielding of $TeO_2$-$B_2O_3$-PbO glass system. *Journal of Radiation and Nuclear Applications*, *6*, pp.31-38.

[13] Sayyed, M.I., Dwaikat, N., Mhareb, M.H.A., D'Souza, A.N., Almousa, N., Alajerami, Y.S.M., Almasoud, F., Naseer, K.A., Kamath, S.D., Khandaker, M.U. and Osman, H., **2022.** Effect of $TeO_2$ addition on the gamma radiation shielding competence and mechanical properties of boro-tellurite glass: an experimental approach. *Journal of Materials Research and Technology*, *18*, pp.1017-1027.

[14] Hussein, K.I., Alqahtani, F.F., Alqahtani, M.S., Alzahrani, K.J., Zahran, H.Y., Alshehri, A.M., Yahia, I.S., Reben, M., Alqahtani, A.M. and Yousef, E., **2022.** Optical and radiation shielding properties for novel glass material: $TeO_2$/$Nb_2O_5$/$Ta_2O_5$/$La_2O_3$. *Chalcogenide Letters*, *19*(6).

[15] Shaaban, K.S., Alomairy, S. and Al-Buriahi, M.S., **2021.** Optical, thermal and radiation shielding properties of $B_2O_3$–NaF–PbO–BaO–$La_2O_3$ glasses. *Journal of Materials Science: Materials in Electronics*, *32*(21), pp.26034-26048.

[16] Takebe, H., Nageno, Y. and Morinaga, K., **1994.** Effect of network modifier on spontaneous emission probabilities of $Er^{3+}$ in oxide glasses. *Journal of the American Ceramic Society*, *77*(8), pp.2132-2136.

[17] Judd, B.R., **1962.** Optical absorption intensities of rare-earth ions. *Physical review*, *127*(3), p.750.

[18] Ofelt, G.S., **1962.** Intensities of crystal spectra of rare-earth ions. *The Journal of Chemical Physics*, *37*(3), pp.511-520.

[19] Carnall, W.T., Fields, P.R. and Rajnak, K., **1968.** Electronic energy levels of the trivalent lanthanide aquo ions. III. $Tb^{3+}$. *The Journal of Chemical Physics*, *49*(10), pp.4447-4449.

[20] Caird, J., DeShazer, L. and Nella, J., **2003.** Characteristics of room-temperature 2.3-μm laser emission from $Tm^{3+}$ in YAG and $YAlO_3$. *IEEE Journal of Quantum Electronics*, *11*(11), pp.874-881.

[21] Babu, P., Seo, H.J., Jang, K.H., Balakrishnaiah, R., Jayasankar, C.K., Lim, K.S. and Lavín, V., **2007.** Optical spectroscopy, 1.5 μm emission, and upconversion properties of $Er^{3+}$-doped metaphosphate laser glasses. *Journal of the Optical Society of America B*, *24*(9), pp.2218-2228.

[22] Assadi, A.A., Damak, K., Lachheb, R., Herrmann, A., Yousef, E., Rüssel, C. and Maâlej, R., **2015.** Spectroscopic and luminescence characteristics of erbium doped TNZL glass for lasing materials. *Journal of Alloys and Compounds*, *620*, pp.129-136.

[23] Pepe, Y., Erdem, M., Sennaroglu, A. and Eryurek, G., 2019. Enhanced gain bandwidth of $Tm^{3+}$ and $Er^{3+}$ doped tellurite glasses for broadband optical amplifier. *Journal of Non-Crystalline Solids*, *522*, p.119501.

[24] Jørgensen, C.K. and Reisfeld, R., **1983**. Judd-Ofelt parameters and chemical bonding. *Journal of the Less Common Metals*, *93*(1), pp.107-112.

[25] Ming, C., Song, F., Yu, Y., Zhang, G., Wang, Q., Yu, H., Sun, T. and Tian, J., **2011.** Optical character of

 © Ariston Publications 2025. All rights reserved.

$Er^{3+}/Yb^{3+}$ co-doped $P_2O_5$–CaO–$Na_2O$–$Al_2O_3$–AgO phosphate glass. *Optics Communications*, *284*(7), pp.1868-1871.

[26] Shi, D.M., Zhao, Y.G., Wang, X.F., Liao, G.H., Zhao, C., Peng, M.Y. and Zhang, Q.Y., **2011**. Effects of alkali ions on thermal stability and spectroscopic properties of $Er^{3+}$-doped gallogermanate glasses. *Physica B: Condensed Matter*, *406*(3), pp.628-632.

ARISTON PUBLICATIONS

© Ariston Publications 2025. All rights reserved. 